Università degli Studi di Ferrara

DOTTORATO DI RICERCA IN
SCIENZE BIOMEDICHE

CICLO XXIV

COORDINATORE Prof. Capitani Silvano

Complex Movements for Voluntary Actions Evoked by Electrical Stimulation in the Motor Cortex of Rats

Settore Scientifico Disciplinare BIO/09

Dottorando
Dott. Bonazzi Laura

Tutore
Dott. Franchi Gianfranco

Anni 2009/2011

A mio figlio Ivan

"Sono le scelte che facciamo
che dimostrano quel che siamo veramente,
molto più delle nostre capacità"

(Albus Silente)

Index

1. Introduction

Electrical intracortical microstimulation (ICMS) has been widely used to study the functional organization of the motor cortex. The ICMS carried out at low level of current with brief trains of electrical pulses (less than 60 ms: short-duration ICMS) have been used to characterize the topographic map of the body in mammal's motor cortex (Asanuma *et al.*, 1976; Donoghue and Wise, 1982). It has been suggested that the body maps in motor cortex attainable through short-duration ICMS was not exhaustive to characterize the complex aspect of the cortical motor control on voluntary movement (Schieber, 2001). Indeed, muscles twitches evoked by short-duration ICMS revealed the strength of synaptic link between cortical neurons and spinal motoneurons, but did cast no light on how motor cortex controlled the activation of spinal motoneurons during natural movement.

The ICMS with longer stimulus trains of about 500 ms (long-duration ICMS) evoked complex and coordinated movement, similar to those of natural behaviour (Graziano *et al.*, 2002). Studies employing long-duration ICMS (Graziano *et al.*, 2002 and 2005) provided evidence that the primate's motor cortex contains in addition to the map of the body, a map of motor repertoire and a map of target locations for the animal hand in the extrinsic space. These maps could span the entire surface of the motor cortex, including primary motor (M1) and premotor areas and could develop overlapped in the same cortical region.

Whether the organizing features of cortical motor control described in primate were consistent across mammals were not completely explored. A previous study in rat (Haiss and Schwarz, 2005) provided evidence that different patterns of motor control are spatially separated and integrated into the whisker motor map suggesting that cortical separation was due to the specific drive of subcortical structures needed to generate different patterns of movement. A recent paper (Ramanathan *et al.*, 2006) have reported that long-duration ICMS in rat motor cortex can result in complex, multijoint forelimb movements organized in a roughly topography. However, since this

study did not examined in detail the topography of evoked movements as it did not provide kinematic informations on evoked movements, it is worthy of interest to define quantitatively the patterns of forelimb movement evoked by long-duration ICMS. The quantitative approach make it possible to verify whether a topography of patterns of movement and a map of target location in space for the limb, can be highlighted in the rat motor cortex.

Guided by these considerations, we pose the question if different features of motor control (e.g. body map, movement patterns, target location in space) can develop overlapping maps in the forelimb region of the rat's M1. We performed long-duration ICMS to evoke complex, multijoint forelimb movements and we used motion analysis tools to measure kinematic variables of electrically-evoked movements.

1.1 Rat motor cortex

In mammals, the hierarchical organization among the cortical motor areas is under investigation. The primary motor cortex (M1) was identified based on its agranular cytoarchitectonic (Brecht *et al.*, 2004). The division between M1 and premotor cortex is notoriously fuzzy: it may be more of a gradient than a border (Graziano *et al.*, 2002). Premotor cortex projects to and controls M1, which in turn projects to and controls the spinal cord. Damage to M1 does not cause a general loss of the ability to move; instead, it results in a specific deficit in fine manual coordination. Many new motor areas have been described, including the supplementary motor area, the cingulated motor areas and many subdivisions of the premotor cortex. However, M1 is the most important region for movement control. It contains a somatotopic representation of the major subdivisions of the body musculature and predominantly controls the limb muscles on the contralateral side of the body albeit only at the level of head, limbs and trunk. Within representations of body parts, M1 map appears to be organized in mostly distributed and overlapping patches (Schieber, 2001). The cortical map of movements is thought to be an emergent property of distributed, horizontal, modifiable network within the cortex (Donoghue, 1995).

In the rat primary motor cortex, the location of major subdivisions, such as the forelimb or hindlimb areas, is somatotopic and is consistent from animal to animal, but the internal organization of the pattern of movements represented within major subdivisions varies significantly between animals. The rat motor cortex includes both agranular primary motor cortex (AgL) and, in addition, a significant amount of the bordering granular somatic sensory cortex (Gr(SI)), as well as the rostral portion of the taste sensory insular or claustrocortex (Cl). The rat frontal cortex also contains a second, rostral motor representation of the forelimb, trunk and hindlimb (see figure below), which is somatotopically organized and may be the rat's supplementary motor area.

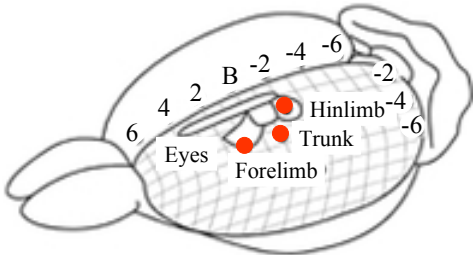

Both of these motor representations give rise to direct corticospinal projections (Neafsey *et al.*, 1985), some of which may make monosynaptic connections with cervical enlargement motorneurons. Medial to the primary motor cortex, in cytoarchitectonic field AgM, is what appears to be part of the rat's frontal eye fields, a region which also includes the vibrissae motor representation. The somatic motor cortical output organization pattern in the rat is remarkably similar to that seen in the primate, whose primary, supplementary and frontal eye field cortical motor regions have been extensively studied.

1.2 Qualisys Optical Motion Capture System

Qualisys Optical Motion Capture is a system developed in Sweden since 1989 and today accepted all over the world. It enables the capture of motion that would be difficult to measure in other ways and it is used in medical and industrial applications. The Qualisys System uses high speed digital cameras (Qualisys ProReflex cameras, see figure below), to precisely capture the motion of a measurement object, with passive or active markers attached. These cameras (complied with the FDA CFR 1040.10 Class I classification) use short but quite strong infrared flashes to illuminate the markers. The flash is generated by LEDs on the front of the cameras. The technology is precise and delivers high quality data to the observer in real-time. The measurement system consists also of high advanced software (QTM) for tracking and analysis of motion data. Software tools perform basic motion calculations such as speed, acceleration, rotations and angles.

1.3 Qualisys Track Manager (QTM)

Qualisys Track Manager is a Windows-based data acquisition software with an interface that allows the user to perform 2D and 3D motion capture. Together with the Qualisys line of optical measurement hardware, QTM streamlines the coordination of all features in a sophisticated motion capture system and provide the possibility of rapid production of distinct and accurate 2D, 3D and 6D data. During the capture, real time 2D, 3D and 6D camera information is displayed allowing instant confirmation of accurate data acquisition. The individual 2D camera data is quickly processed and converted into 3D or 6D data by advanced algorithms, which are adaptable to different movement characteristics. The data can then be exported to analysis software via several external formats.

1.4 Multivariate statistics

Multivariate statistics is a form of statistics encompassing the simultaneous observation and analysis of more than one statistical variable. The application of multivariate statistics is multivariate analysis. Methods of bivariate statistics, for example simple linear regression and correlation, are special cases of multivariate statistics in which 2 variables are involved. Multivariate statistics concerns understanding the different aims and background of each of the different forms of multivariate analysis, and how they relate to each other. The practical implementation of multivariate statistics to a particular problem may involve several types of univariate and multivariate analysis in order to understand the relationships between variables and their relevance to the actual problem being studied. In addition, multivariate statistics is concerned with multivariate probability distributions, in terms of both:

- how these can be used to represent the distributions of observed data;
- how they can be used as part of statistical inference, particularly where several different quantities are of interest to the same analysis.

There are many different models, each with its own type of analysis:

1. Multivariate analysis of variance (MANOVA) extends the analysis of variance to cover cases where there is more than one dependent variable to be analyzed simultaneously: see also MANCOVA;
2. Multivariate regression analysis attempts to determine a formula that can describe how elements in a vector of variables respond simultaneously to changes in others. For linear relations, regression analyses here are based on forms of the general linear model;
3. Principal components analysis (PCA) creates a new set of orthogonal variables that contain the same information as the original set. It rotates the axes of variation to give a new set of orthogonal axes, ordered so that they summarize decreasing proportions of the variation;

4. Factor analysis is similar to PCA but allows the user to extract a specified number of synthetic variables, fewer than the original set, leaving the remaining unexplained variation as error. The extracted variables are known as latent variables or factors; each one may be supposed to account for covariation in a group of observed variables;
5. Canonical correlation analysis finds linear relationships among 2 sets of variables; it is the generalised (canonical) version of bivariate correlation;
6. Redundancy analysis is similar to canonical correlation analysis but allows the user to derive a specified number of synthetic variables from one set of (independent) variables that explain as much variance as possible in another (independent) set. It is a multivariate analogue of regression;
7. Correspondence analysis (CA), or reciprocal averaging, finds (like PCA) a set of synthetic variables that summarise the original set. The underlying model assumes chi-squared dissimilarities among records (cases). There is also canonical (or "constrained") correspondence analysis (CCA) for summarising the joint variation in 2 sets of variables (like canonical correlation analysis);
8. Multidimensional scaling comprises various algorithms to determine a set of synthetic variables that best represent the pairwise distances between records. The original method is principal coordinates analysis (based on PCA);
9. Discriminant analysis, or canonical variate analysis, is a statistical analysis to predict a categorical dependent variable by one or more continuous or binary independent variables and it is useful in determining whether a set of variables is effective in predicting category membership;
10. Linear discriminant analysis (LDA) computes a linear predictor from 2 sets of normally distributed data to allow for classification of new observations;
11. Clustering systems assign objects into groups (clusters) so that objects (cases) from the same cluster are more similar to each other than objects from different clusters;

12. Recursive partitioning creates a decision tree that attempts to correctly classify members of the population based on a dichotomous dependent variable;
13. Artificial neural networks extend regression and clustering methods to non-linear multivariate models.

There is a set of probability distributions used in multivariate analyses that play a similar role to the corresponding set of distributions that are used in univariate analysis when the normal distribution is appropriate to a dataset. These multivariate distributions are:

- Multivariate normal distribution;
- Wishart distribution;
- Multivariate Student-t distribution.

1.5 Tukey's test

Tukey's test, also known as the Tukey range test, Tukey method, Tukey's honest significance test, Tukey's HSD test (Honestly Significant Difference test) (Lowry, 2008), or the Tukey–Kramer method, is a single-step multiple comparison procedure and statistical test generally used in conjunction with an ANOVA to find which means are significantly different from one another. Named after John Tukey, it compares all possible pairs of means, and is based on a studentized range distribution q (this distribution is similar to the distribution of t from the t-test) (Linton *et al.*, 2007). The test compares the means of every treatment to the means of every other treatment; that is, it applies simultaneously to the set of all pairwise comparisons μ_i - μ_j and identifies where the difference between 2 means is greater than the standard error would be expected to allow. The confidence coefficient for the set, when all sample sizes are equal, is exactly $1 - \alpha$. For unequal sample sizes, the confidence coefficient is greater than $1 - \alpha$. In other words, the Tukey method is conservative when there are unequal sample sizes. Tukey's test is based on a formula very similar to that of the t-test. In fact, Tukey's test is essentially a t-test, except that it corrects for experiment-wise error rate (when there are multiple comparisons being made, the probability of making a type I error increases. Tukey's test corrects for that, and is thus more suitable for multiple comparisons than doing a number of t-tests would be) (Linton *et al.*, 2007).

The formula for Tukey's test is:

$$q_s = \frac{Y_A - Y_B}{SE}$$

where Y_A is the larger of the 2 means being compared, Y_B is the smaller of the 2 means being compared, and SE is the standard error of the data in question.

This q_s value can then be compared to a q value from the studentized range distribution. If the q_s value is larger than the $q_{critical}$ value obtained from the distribution, the 2 means are said to be

significantly different. Since the null hypothesis for Tukey's test states that all means being compared are from the same population (i.e. $\mu_1 = \mu_2 = \mu_3 = ... = \mu_n$), the means should be normally distributed (according to the central limit theorem). This gives rise to the normality assumption of Tukey's test. The Tukey confidence limits for all pairwise comparisons with confidence coefficient of at least 1 − α are:

$$\bar{y}_{i\bullet} - \bar{y}_{j\bullet} \pm \frac{q_{\alpha;r;N-r}}{\sqrt{2}} \widehat{\sigma}_\varepsilon \sqrt{\frac{2}{n}} \qquad i, j = 1, \ldots, r \quad i \neq j.$$

Notice that the point estimator and the estimated variance are the same as those for a single pairwise comparison. The only difference between the confidence limits for simultaneous comparisons and those for a single comparison is the multiple of the estimated standard deviation. Also note that the sample sizes must be equal when using the studentized range approach.

$\widehat{\sigma}_\varepsilon$ is the standard deviation of the entire design, not just that of the 2 groups being compared. The Tukey–Kramer method for unequal sample sizes is as follows:

$$\bar{y}_{i\bullet} - \bar{y}_{j\bullet} \pm \frac{q_{\alpha;r;N-r}}{\sqrt{2}} \widehat{\sigma}_\varepsilon \sqrt{\frac{1}{n_i} + \frac{1}{n_j}}$$

where n_i and n_j are the sizes of groups i and j respectively. The degrees of freedom for the whole design is also applied.

The Tukey method uses the studentized range distribution defined as:

$$q_{r,\nu} = w/s.$$

Tukey's test is based on the comparison of 2 samples from the same population. From the first sample, the range (calculated by subtracting the smallest observation from the largest, or range = $max_i\ (Y_i) - min_i\ (Y_i)$ where Y_i represents all of the observations) is calculated, and from the second sample, the standard deviation is calculated. The studentized range ratio is then calculated:

$$q = \frac{\text{range}}{s}$$

where q = studentized range, and s = standard deviation of the second sample.

This value of q is the basis of the critical value of q, based on 3 factors:

1. α (the type I error rate, or the probability of rejecting a true null hypothesis);
2. n (the number of degrees of freedom in the first sample (the one from which range was calculated);
3. v (the number of degrees of freedom in the second sample (the one from which s was calculated);

The distribution of q has been tabulated and appears in many textbooks on statistics.

If there are a set of means (A, B, C, D), which can be ranked in the order $A > B > C > D$, not all possible comparisons need be tested using Tukey's test. To avoid redundancy, one starts by comparing the largest mean (A) with the smallest mean (D). If the q_s value for the comparison of means A and D is less than the q value from the distribution, the null hypothesis is not rejected, and the means are said have no statistically significant difference between them. Since there is no difference between the 2 means that have the largest difference, comparing any 2 means that have a smaller difference is assured to yield the same conclusion (if sample sizes are identical). As a result, no other comparisons need to be made (Linton *et al.*, 2007).

Overall, it is important when employing Tukey's test to always start by comparing the largest mean to the smallest mean, and then the largest mean with the next smallest, etc., until the largest mean has been compared to all other means (or until no difference is found). After this, compare the second largest mean with the smallest mean, and then the next smallest, and so on. Once again, if 2 means are found to have no statistically significant difference, do not compare any of the means between them (Linton *et al.*, 2007). If only pairwise comparisons are to be made, the Tukey–Kramer method will result in a narrower confidence limit (which is preferable and more powerful) than Scheffé' method.

2. Materials and Methods

A total of 7 male Albino rats, weighing 280-330 g were used to characterize the forelimb movement evoked by a long-duration intracortical stimulation (ICMS) and to perform a quantitative analysis of kinematics of these complex movements. Other 7 animals were used in pilot studies whose data were not included in the paper. The experimental plan was designed in compliance with Italian Law regarding the care and use of experimental animals (DL116/92) and approved by the institutional review board of the University of Ferrara and by the Italian Ministry of Health. For all experimental procedures rats were anesthetized initially with ketamine HCl (80 mg/Kg i.p.). For the duration of the experiment, anesthesia was maintained by supplementary ketamine injections (4 mg/Kg i.m given as required, typically every 25-30 minutes) so as to achieve long-latency and sluggish hindlimb withdrawal upon pinching the hindfoot. Under anesthesia, the body temperature was maintained at 36-38° with a heat lamp.

2.1 Long-duration Intracortical Microstimulation

ICMS mapping was aimed at defining the topographic distribution of complex forelimb movement in M1. The mapping procedure was similar to the one described by Ramanathan *et al.* (2006) in the rat and Graziano *et al.* (2002) in the monkey. The animals were placed in a Kopf stereotaxic apparatus and the frontal cortex of one hemisphere was exposed by a large craniotomy. The dura remained intact, and was kept moist with saline solution. The electrode penetrations were regularly spaced out over a 500 μm grid. Alteration in the coordinate grid, up to 50 μm, were sometimes necessary to prevent the electrode from penetrating the surface blood vessels. Glass insulated tungsten electrodes (0.6-1 MΩ impedance at 1 kHz) were used for stimulation. The electrode was lowered vertically to 1.5 mm below the cortical surface and adjusted ± 200 μm so as to evoke movement at the lowest threshold. In a previous experiment this depth was found to correspond to layer V of the frontal agranular cortex (Franchi, 2000).

To identify complex movements, at each cortical site studied, stimulation will be applied by an S88 stimulator (Grass) and 2 PSIU6 stimulus isolation units (Grass, Quincy, Mass., USA). A 500 msec train of 200 μsec duration bipolar pulses will be delivered at 333 Hz. Each stimulation pulse was a negative followed by a positive phase; bipolar pulses were used to minimize damage that may occur during long-duration stimulation (Graziano *et al.*, 2002). Current was measured by the voltage drop across a 1 KOhm resistor in series with the return of the stimulus isolation units. At each cortical site, the stimulating current was increased gradually until a clear multijoint movement of the forelimb was detected. The threshold, the current at which the movement was evoked 50% of the time, was determined by 2 observers. Once a movement threshold was detected, the current was raised up to 100 μA to optimize that movement and ease its characterization, and the quantitative testing was begun. In some cases we change the stimulation parameters to value their effects on multijoint movements. If no movement was detected up to 100 μA, the site was defined as 'non-responsive'.

2.2 Evoked movements characterization and complex movements map construction

Movements evoked by long-duration ICMS were visually identified during mapping sessions and videotaped at 30 frames/sec by a standard camera. Evoked movements were examined and recorded with the animal supported in a fixed position in an elevated stereotaxic frame (Kopf). The body of the animal was laid on a table in a prone position with its forelimbs hanging down and free to move in all direction against gravity. The position of the trunk was stabilized to the back of the table to minimize spontaneous trunk movements (head/chest-fixed coordinates). The rest position for each forelimb was in approximately half-way extension-adduction and the wrist rested palm down, with the finger joints in semi extension (see Fig. 1A).

The recording video camera was positioned so as obtain a lateral or a frontal view of the animal. In order to detect the starting of the stimulus a triggered led was located near the body of the animal within the visual field of the camera. The video recording served as a back-up to clarify the data

analysis and gave information of the occurrence of the forelimb movements. Videotaped movements were analyzed frame-by-frame by using Quicktime and iMovie software.

2.3 Kinematic recording of complex movements and analysis

Movements evoked by long-duration ICMS were recorded and measured with a motion 3D optical analyzer (Qualisys Motion Capture System; Qualisys North America Inc., Charlotte, USA). 2 adhesive infrared-reflective spheres (diameter: 0.4-0.3 cm, weight: 0.04-0.05 g) were placed as a markers, on the forelimb skin over 2 anatomic landmarks: the wrist (head of the ulna), used to detect the limb movement and the last-phalangeal joint (tip) of the middle digit, used to detect the paw movement (Fig. 1A). The motion analysis system provided the 3D coordinates of the markers in space and it was then possible to reconstruct the ICMS-evoked movements. In order to minimize variability in marker positioning, markers in all experiments were placed by the same operator. 3 infrared cameras, placed around animals, were used to record position of markers (Fig. 1B). The cameras calibration has been conducted according to the Qualisys Motion Capture Analysis System proceedings. To do this, a stationary L-shaped reference structure with 4 markers attached to it placed under animals (see figure below and also Fig. 1A: box at the top right) defined the origin and orientation of the 3D coordinate system.

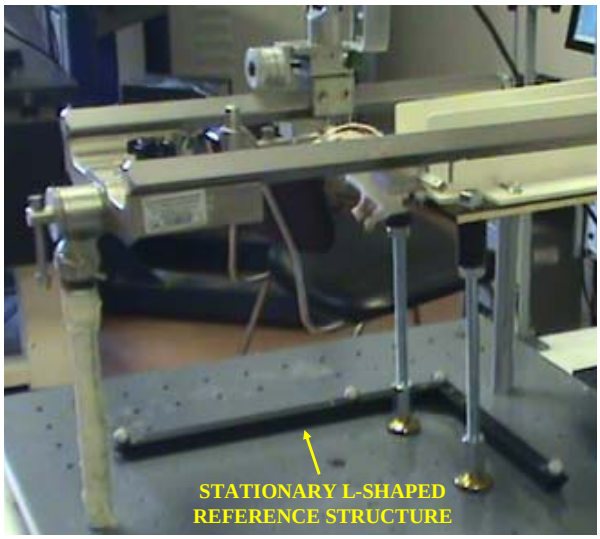

The direction of coordinate X-, Y- and Z-axis was anterior, lateral and vertical respectively. Movements were recorded for 2 seconds at a sampling rate of 100 Hz. Kinematic data will be analyzed off-line with Qualisys Track Manager software and with custom MATLAB programs to extract kinematic features. Recording trials were not considered for analysis when the fill level of recording was < 100%. This amounted to less than 15% of all trials. The start position of the forelimb was never modified during repetitive stimulations and recordings. Before each recording session, minor modifications of the forelimb positions were corrected to obtain the optimal visibility of the 2 markers within the calibrated field of the cameras. The purpose was to stimulate at the moment when the forelimb remained stationary in position of rest, so all stimulation trials took place in absence of spontaneous movement. In all animals, sham stimulation trials were recorded both while the animal was standing quietly with the forelimb stationary and while moving it spontaneously. The pattern obtained during sham stimulation was therefore unlike the pattern obtained during cortical stimulation at that site and unlike the pattern found at any stimulated site. Some spontaneous forelimb movement was observed at rest, however, in order to avoid interference between the evoked and spontaneous movement, a movement was detected as a displacement in XYZ-axes over a distance exceeding 5 mm. All measures was performed by subtracting the marker's rest position in Cartesian coordinates from all points along the trajectory, thus all data sets began at (0,0,0). At first, the analysis was aimed to define the classes of movement and their topography across the cortical surface. Then, various kinematic parameters related to the limb and the paw component were determined from the analysis of the wrist and the digit marker separately and with different constrains. Moreover, the digit marker was evaluated in relation to the wrist marker.

Since a vertically component (Z-axis) was found in all evoked limb movements, the maximal displacement in one of the XY-axes defined the limb class of movement when it was over a distance exceeding 15% of the displacement in other axis. The displacement in Z-axis defined the type of movement when the displacement in XY-axes was < 5mm. We found that these values were

the most reliably to define the type of limb movement in all animals. When a displacement of both markers was observed the paw component of the movement was obtained by subtracting the wrist marker value to the digit marker value from all points throughout the movement. Thus, data sets of digit marker were defined by:

actual measures of digit markers values - actual measures of wrist marker values

In order to avoid interference between active and passive (transport limb depended) digit movement, a paw movement was detected as a displacement in 2 of the XYZ-axes over a distance exceeding 5 mm.

We computed the following kinematic parameters:

- Maximal displacement in XYZ (MD:X,Y,Z);
- Movement latency (L);
- Movement duration (D);
- Maximum peak velocity (MPV);
- Mean velocity (MV);
- Number of peak velocity (PV);
- Trajectory (T);
- Displacement vector (DV);
- Path index (PI).

The start of movement (L) was defined by the frame at which the tangential velocity exceeded 5% of maximum velocity (Adamovich *et al.*, 2001). The end of movement was defined by the last frame at which the marker reached the maximal displacement in one of the XYZ-axes. In this way the displacement toward the resting position and outlasting the stimulus was always outside the movement duration. All kinematic variables were calculated from the start to the end of movement (D). We determined the trajectory (T) and displacement vector (DV) from initial to final limb position for each stimulated site. Limb trajectory straightness was determined by the path index (PI) defined as the ratio of T/DV. Using this measure, a limb trajectory equal to a straight line has an

index of 1 while the equal to a semicircle has an index of 1.57 (Archambault *et al.*, 1999). In any case, a path index of greater than 1.57 represent either an S- or C- shaped or coil-like shape in sequences of movement. T and DV were used to determine the end-point 3D location of the limb, so they were considered only for the wrist marker. The number of peaks (PV) within the speed profile has been used to quantify the forelimb movement smoothness. Since the mean speed of movement was lower than its peaks, we count a pick when it was over the mean speed of the movement. In this study, peaks in speed represent decreases in smoothness or periods of acceleration and deceleration of movements evoked by a long-duration electrical stimulus. For each stimulated site the kinematic variables were obtained by averaging the values attained in 2-5 microstimulation trials.

2.4 Data presentation and statistical analysis

We used Multivariate Discriminant Analysis (MDA; Barker and McCombe, 1999) in order to analyse the displacement in XYZ-axes and kinematic variables for classifying movements in predefined classes. This method for analysing time-series biomechanical data allowed to determine the class of movement based on a set of variables known as predictors or input variables. The measure of confidence that the classification was correct and the measure of the predicted error rate on each classification were defined by:

- Proportion Correct = number of correctly classified samples/ total number of samples;
- Error Rate = number of rejected samples/ total number of samples.

All individual displacements in XYZ-axes, were also plotted in 2D space (Fig. 3 and Fig. 8) to evaluate their spatial dispersions. To characterize the spatial distribution of all movements in the motor cortex across animals, a 2D distribution of movement-responsive sites at coordinate relative to bregma was generated. Each movement-related site was taken to represent a square of 0.25 mm^2 of cortical surface (0.5X0.5 mm) and 100% of probability in one site was achieved when a movement at that site was observed in all 7 animals (Fig. 4 and Fig. 9). We used the spherical

coordinate system (Fig. 1C) for physical 3D space evaluation of limb movement direction. Spherical coordinates is a coordinate system for 3D space where the position of a point is specified by 3 numbers:

- *rho*: is the distance of a point P from the origin. In present data *rho* was the limb movement vector length of value greater than 0;
- *phi*: was the angle between the X-axis and the ray between the projection of P onto the XY-plane and the origin; counter clockwise was considered the positive direction (*phi*: between 0 and ±180°)*;*
- *theta*: was the angle between the Z-axis and the ray from the origin to P (*theta:* between 0 and 180°).

Multivariate test for difference in means (MANOVA) was used to compare displacement in XYZ-axes and kinematic variables. To analyze differences in kinematic means between classes of movement, one-way ANOVA followed by Tukey's test were performed. Pearson correlation (r) significant at the 0.05 level was used to assess the relationship between kinematics variables. The reproducibility of kinematic measures between trials of repeated measures, was obtained calculated the coefficient of variation (CV = standard deviation/mean). All statistical procedures were performed in Minitab15 Statistical software features and in MATLAB (R2006a) applications for statistics and data analysis.

3. Results

Altogether, 339 sites were stimulated in the motor cortex of one hemisphere of 7 rats. The 41% of these sites was not considered for the result, since no markers displacement was evoked or the displacement in XYZ-axes was less than 5 mm (see Methods). Usually, these sites were located on the outskirts of the forelimb region delineating its border. In addition, forelimb movement were observed simultaneously with non-forelimb movements, as vibrissa, neck, hindlimb or mouth, near the borders between the forelimb area and these respective representations. In all animals, forelimb movements on the controlateral body side to the stimulated hemisphere were evoked. In addition some stimulated site evoked bilateral movements. At no site were forelimb movement evoked exclusively on the side ipsilateral to stimulating electrode. The mean stimulation threshold for evoking movements was 46.52 ± 2.36 μA. To facilitate the movement characterization, without altering its quality, all recordings were performed at 100 μA. The evoked movement proved to be repeatable from trial to trial and their features remained nearly constant over the time required to characterize each cortical site. Figure 2 shows a representative example of surface map of forelimb movements evoked by long-duration ICMS. In this scheme each of the forelimb site was characterized by movement of one or both markers. Overall, the limb movement (wrist marker) was evoked in 38.0% of sites, the paw movement (digit marker) was evoked in 11.5% of sites, and the limb-paw movement (both markers) was evoked in the remaining 50.5% of sites. A topography of complex movements was found, including the presence of 2 distinct forelimb areas (caudal and rostral forelimb area) in many cases not well separated from each other.

3.1 Stimulation-evoked limb (wrist marker) movements

Long-duration ICMS elicited wrist marker movement in 177 out of 200 sites. Since a vertically component (Z-axis value > 5 mm, see Methods) was found in all evoked movements, we have classified movements according to the maximal displacement (MD) on the X or Y axis. According to MD (Tab.1), the repertoire of the limb movement included: abduction (*ab*, 55,37%, MD Y-axis positive), adduction (*ad*, 10,17%, MD Y-axis negative), extension (*ex*, 19,77%, MD X-axis positive), retraction (*rt*, 1.7%, MD X-axis negative) and elevation (*el*, 12.99%, Z-axis positive and X and Y axes < 5mm). The Multivariate Discriminant Analysis (MDA) classifier achieved an 88.1% correct classification rate with inputs of class of movement vs XYZ value. This indicates that 88.1% of the limb movements were assigned to the correct class (156 out of 177; $P < 0.0001$, MANOVA for XYZ vs Movement Class); 11.9% of false alarm rate was due to some *ab* (11 out of 98) and *ex* (6 out of 35) movements that the MDA classifier recognized as *el* movements. When all individual displacements were plotted in 2D space, classes of movement were highlighted as a cluster of points in the scatter plot of MD: X vs Y (Fig. 3A), conversely, the clusters of points were not well separated in the scatter plot of MD: X vs Z and MD: Y vs Z (Fig. 3B-C). Overall, these quantitative analysis suggested that movements were correctly classified. To characterize the spatial distribution of classes of movements in motor cortex across animals, a 2D frequency distribution bregma relative of limb-responsive sites was generated. Figure 4 showed a consistent topography in which cumulative sites were coded according to their rate. In this arrangement of stimulated effects, *ab*-related sites were clustered more posteriorly at coordinate corresponding the caudal forelimb region, *ad*-related sites were clustered more anteriorly at coordinate corresponding to the rostral forelimb region, *ex*-related sites were clustered at coordinate corresponding to the rostral forelimb region and the anterior part of the caudal forelimb region. The *rt*-related sites, was found to span the posterior border of the forelimb motor region. Unlike to other sites, *el*-related sites were scattered over the forelimb motor region so no overall topography was apparented. To evidence whether the topography of movements across cortical surface was associated with another

dimension of topography with respect to the limb direction, the sites were categorized according to their spatial end-points. The figure 5A showed an example of final end-points spatial map, derived from 1 animal. We have expressed the degree of spatial convergence in each stimulation site by calculating the coefficient of variation of the end-point coordinate. For each stimulation site, the coefficient of variation was expressed as the average of values from trial to trial (see Methods). The range of end-points variation in XYZ-axes among stimulated sites was 0.003-0.041, and the average coefficients of variation was 0.02 ± 0.019. This low values indicated that the stimulation in each site caused a significant spatial convergence of the limb toward a target location. To characterize the end-points spatial distribution across animals, we defined the vector movement spatial position in a 3D spherical coordinate system. In this system, each movement vector was made to origin from the intersection of axes while its length (*rho*) with the 2 angles (*theta* and *phi*), defined the final position of the wrist marker (Fig. 1C). Since *el* movements were carried out vertically upwards with negligible XY displacement, they were not considered for this computation. The MDA analysis confirmed the convergence for each class of movement toward a region of space in 3-Cartesian dimensions (Predictors: *rho* (mm)- *theta*- *phi* (grad) vs Movement class, N. correct: 137 out of 154, Proportion Correct = 0.89; $P < 0.0001$, MANOVA). This convergence can be seen in grater detail in the scatter plot of *phi* vs *theta* and *phi* vs *rho* (Fig. 5B-C), conversely there was no clear spatial clustering between the class of movements in the plot of *theta* vs *rho* (Fig. 5D). These results showed that similar spatial map of end-points was a consistent feature of the limb motor cortex in all mapped animals, and suggested that the spatial map of the limb movement was strongly related to the azimuthal (latitude) component of the movement in the 3-Cartesian dimension.

3.2 Limb (wrist marker) movements kinematics

Table 2 sums up the kinematic variables calculated from the wrist marker during the limb movement. A significant interaction was observed for movement latency and duration (L: $F_{(4,175)} = 5.06$, $P = 0.001$; D: $F_{(4,176)} = 3.78$, $P = 0.006$) between the class of movements. As shown by post-hoc analysis, *ab* movement had a significant shorter latency ($T = 4.16$, $P = 0.0005$) and longer duration ($T = -2.98$, $P = 0.026$) when compared to *ad* movement. With regard to the velocity variables, no significant effect of class was found for maximum velocity, conversely, a significant interaction was found between class for mean velocity (MV: $F_{(4,172)} = 2.66$, $P = 0.035$) and peak velocity number (PV: ($F_{(4,176)} = 11.74$, $P < 0.0001$). It was found that the *ex* movement showed a significant higher MV ($T = 3.85$, $P = 0.026$) compared to *el* movement and a significant higher PV compared to *ab* ($T = 6.34$, $P < 0.0001$), *ad* ($T = 5.3$, $P < 0.0001$) and *el* movement ($T = 3.85$, $P = 0.002$) while *ab*, *ad* and *el* movements did not significantly differ from each other in these respect. There was found to be a highly significant main effect of class on trajectory length (T: $F_{(4,176)} = 13.10$, $P < 0.0001$) and vector length (DV: $F_{(4,176)} = 26.72$, $P < 0.0001$). The post-hoc test revealed that the class differences found by means of T and DV, were mainly related to the fact that *ab* and *ex* movement had significantly greater value in both T and DV in comparison to other class of movements (all comparisons: $P < 0.0001$). Furthermore the post-hoc comparison revealed that *ab* movement significantly different from *ex* movement in virtue of shorter T ($T = 3.34$, $P < 0.009$) and longer DV ($T = -3.96$, $P < 0.002$). We tried to estimate whether the trajectory lengths were consistent trial by trial in each stimulated site. On repeated trials with the same stimulation parameters, the average coefficient of variation (SD/mean) of T was 0.17 ± 0.1 (range: 0.01-0.32). Then we have evaluated the ICMS-evoked T degree of straightness, using the path index (PI: see Methods). All trajectories had a curved shape ($PI > 1$) and only the 32.9% had a PI below 1.57. The trajectories with a $PI > 1.57$ exhibited a general C- or S-like shape, while only the 6% had a coil-like shape (Fig. 6). Notably, coil-like trajectory were found only in the 25.7% of *ex* movements. In agreement with this finding, the *ex* movement showed a PI number of 3.72, significantly and

considerably greater that other movement PI ($F_{(4,176)} = 9.89$, $P < 0.0001$). The correlation analysis was used to describe the relationship between multiple kinematic variables presented in the Table 2. Correlations were positive between D and T ($r = 0.18$, $P = 0.01$) and DV ($r = 0.265$, $P < 0.0001$) conversely, correlations were negative between L and D ($r = -0.23$, $P = 0.002$) and DV ($r = -0.41$, $P < 0.0001$). There was a strong positive correlation between T and kinematic variables of velocity (MV: $r = 0.4$, $P < 0.0001$; MPV: $r = 0.57$, $P < 0.0001$) and the PV ($r = 0.58$, $P < 0.0001$).

3.3 Stimulation-evoked paw (digit marker) movements

It was observed ICMS-evoked digit marker movement in 124 sites out of 200 sites. As can be seen from the video sequences (Fig. 7) and MD values (Tab. 3), paw movements included: opening (*O*: 66.1%, MD X positive), closure (*C*: 5.6%, MD X negative), opening/closure sequence (*OCs*: 9.7%, opening phase MD X positive, followed by closing phase, MD X negative) and supination (*S*: 18,5% MD Z positive). We asked whether opening and closing phase in *OCs* were different from *O* and *C* movement, respectively. The MDA classifier achieved an 73.9% correct classification rate with inputs of class of movement vs XYZ value (N. correct: 137 out of 154; $P < 0.0001$, MANOVA). The false alarm rate (26.1%) was largely due to the low discrimination between *O* and the OC_S opening phase (*O* Proportion Correct: 0.67; opening phase of *OCs* Proportion Correct: 0.58). Conversely, MDA classifier achieved a 100% classification rate for *C* and the *OCs* closing phase. All these aspects of paw movements, can be seen in greater detail when all individual displacements were plotted in 2D space. As showed in the Fig. 8, the clusters of points were not well separated in the MD plot of X vs Y (Fig. 8A), conversely, classes of movement were clearly clustered in MD plot of X vs Z (Fig. 8B). Notably, the overlap of *O* and *OCs* opening phase points in all 3 plots. *O*, *C*, and *OCs* movements characterized by simultaneously digits contraction; *S* movement characterized by wrist external rotation without fingers movement. Moreover, *O*, *C*, and *S* movements appeared as a single movement in each single trial, conversely, the *OCs* movement characterized by repetitive sequences of opening and closing phase in each single trial (mean of

sequences: 5.03 ± 0.5, range 4-8). Thus, these analysis together suggested that *O*, *C*, *OCs* and *S* were different classes of paw movement. The bregma relative frequency distribution of paw-responsive sites showed a consistent topography of class of movement across the cortical surface (Fig. 9). The *O* movement was elicited in a portion of the forelimb region, where the stimulation most often elicited *ab* movement while the *C* and *OCs* movement was elicited in a portion where the stimulation most often elicited *ad* or *ex* movement. Finally, the *S* movement was elicited in a more lateral portion of the forelimb region where limb movement was less commonly elicited by electrical stimulation.

3.4 Paw (digit marker) movement kinematics

Table 4 sums up the kinematic variables calculated from the wrist marker during the paw movement. The MDA classifier achieved a high level of classification rate with input of kinematic variables vs class of movement (Predictors: Kinematic variables vs Movement Class, N. correct: 98 out of 124, Proportion Correct = 0.79; $P < 0.0001$, MANOVA). All paw movements began at short latency after the stimulation (L mean: 27.47 ms) and no significant difference in L between the classes of movement has been detected ($F_{(3,123)} = 0.92$, $P = 0.43$). There was no significant difference in D between *O*, *C* and *S* movements (all comparisons $T > 0.5$, $P > 0.7$); conversely, the *OCs* movement had longer D in comparison to other classes of movement (all comparisons $T > 4.9$, $P < 0.0001$). With regard to the MV, the *C* movement proved faster than the *O* movement (MV: $T = 3.01$, $P = 0.017$). In *OCs* movement the PV was significantly higher than the other classes of movement (all comparisons: $T > 12.1$, $P < 0.0001$) that did not significantly differ from each other in this respect (all comparisons: $T < 0.1$, $P > 0.9$). Notably, in *OCs* movement, PV were at the opening phase of the movement. Finally, *S* movement proved much slower than movements involving the fingers (all comparisons, MPV: $T > 3.5$, $P < 0.004$, MV: $T > 4.17$, $P < 0.0001$).

3.5 Relation between limb and paw movement

Limb-paw movements accounted for half of all stimulation-induced forelimb movement (101 out of 200 sites). There was no clear topography of sites that showed limb-paw movement and sites that did not; both types of sites were intermingled in cortex. A specific pattern of limb and paw movement combination existed. Specifically, *O* movement was combined with the *ab* movement (63.4%), *ex* movement (18.3%) or *el* movement (18.3%). With regard to the placement of the maximum paw opening as a percent of the total limb movement, it was found that the paw maximum opening occurred at 73.0% of *ab* movement and at 100.3% and 95.7% of *ex* and *el* movement, respectively. Note that, the *O* movement duration did not change when it was combined to *ab*, *ex* or *el* movement ($F_{(2,81)} = 0.51$, $P = 0.601$). The *C* movement was always combined with *ad* movement and its maximum closure occurred at 191.0% of *ad* movement. The 28.64% of *ad-C* movements involved a time-synchronized mouth opening. The *OCs* movement was always combined with *ex* movement and sequences occurred over 135.69% of the time needed for the *ex* movement. There was also found that in the *ab-O* movement, the *ab* had a significant shorter latency in comparison to *O* (*ab* vs *O*: 24.04 vs 29.62 ms; $F_{(1,103)} = 7.75$, $P = 0.006$). In other limb-paw movement combinations the latency value was equal in both the limb and paw component then, in these movements the motions at the involved joints began almost simultaneously.

4. Discussion

In the discussion of this doctoral thesis, we have the goal of showing how the long-duration ICMS has the potential to reveal a better characterization of the organization of the forelimb motor cortex in the mammals and specifically, how it is useful for understanding the strategy governing the organization of the forelimb map in rat's motor cortex.

Our findings have shown that long-duration stimulation paradigms result in reproducible activation of groups of forelimb muscles to achieve complex movements which may be set out in terms of their kinematic properties. The electrically-evoked movements were described in terms of 3D displacement and kinematics variables recorded from 2 markers positioned on the wrist and middle digits of rat's forelimb. The results confirmed and extended previous findings that have documented the existence of complex movement representations within the motor cortex of monkeys (Graziano *et al.*, 2002; Gharbawie *et al.*, 2011; Stepniewska *et al.*, 2011) and rats (Ramanathan *et al.*, 2006). The quantitative analysis of markers separately allowed to define 5 classes of limb movements (*ab, ad, ex, rt, el*) and 4 classes of paw movements (*O, C, OCs, S*). In half of all forelimb-related stimulated sites a specific pattern of limb and paw movement combination existed. The present finding provide insight regarding internal organization and distribution of patterns of complex movement in the rat's forelimb motor cortex.

4.1 Methodological and Technical remarks

In this study, the long-duration ICMS was combined with the motion 3D analysis of the ICMS-evoked forelimb movement. To our knowledge, this is the first study to use the motion analysis to asses the reproducibility of kinematic measures of ICMS-evoked complex forelimb movement in rats. The idea of combining these techniques might be well suited when motor cortical output is intended to be quantified and components of ICMS-evoked movement (limb and paw movement) have to be objectively assessed and documented. Because the markers were attached at the wrist

and middle digits, it was predicted that the limb and paw movement had a large prevailing effect on wrist and digit marker, respectively. This allows the investigation of whether the subcomponents of complex movement follows a gradient into the rat's forelimb motor cortex. To this end, a 3D recording system generally used to record kinematics in humans and monkeys has been adapted to recording kinematics in rats. The system our group used for kinematic assessment of forelimb movements was an infrared-based motion analyzer. Alternative systems used ultrasound, electromagnetic or video-based signals to investigate the spatio-temporal characteristics of forelimb movement. All systems appear to have comparable sensitivity and reliability. An advantage of infrared reflecting markers was that this system work wireless and is easily interfaced with a video camera and with data processing systems. Moreover, this system has proved suitable to record kinematics with small neighbours markers on a small forelimb. Rats were suitably positioned on the stereotactic system within the calibrated space to obtain stable and reproducible kinematic measures on repeated recordings and to establish a range of values for reliability of kinematic measures. Here we used conditions in which the full expression of neural, muscular, and biomechanical occurred. The evoked forelimb movements were made against gravity, as would natural movement, although the forelimbs hanging position with the head fixed to the stereotactic under anaesthesia was not a natural setting.

Asanuma and Arnold (1975) found that trains of cathodal pulses killed the cortical tissue around the electrode tip. With balanced biphasic pulses it is possible to stimulate for long durations and high current without measurable damage (Theovnik, 1996). Our stimulation paramenters are within the range of cortical stimulation studies in oculomotor, visual, and sensory-motor system (Bruce *et al.*, 1985; Freedman *et al.*, 1996; Gottlieb *et al.*, 1993; Romo *et al.*, 1998; Salzman *et al.*, 1990; Tehovnik and Lee, 1993). Finally, in present experiments using the same stimulation techniques in rat, on histology no visible damage to the cortex associated with the stimulation was found.

How much did the effects of ketamine anaesthesia contribute to the patterns of evoked movement observed in the present study?

Ketamine takes effect by selective blockade of NMDA receptors leaving fast transmission by AMPA and, notably, GABA receptors intact (Ebert *et al.*, 1997; Sonner *et al.*, 2003). In contrast to other anaesthetics, the spontaneous firing rate and sensory evoked cortical activity are enhanced (Kayama *et al.*, 1972) and a comparable pattern of cortical excitation and inhibition after ICMS was observed in ketamine-anaesthetized and awake animals (Butovas and Schwarz, 2003). Moreover, in the ketamine-anaesthetized animals, stretch reflexes, flexion reflexes, and reciprocal inhibition between antagonistic muscles are manifest (Capaday *et al.*, 1998; Schneider *et al.*, 2001). Thus, in the present experimental condition, we characterized how activation of corticospinal inputs to the spinal cord activated from separated sites of motor cortex produced patterns of motor output. Supports for this notion comes from the finding of very similar motor patterns of vibrissae movement in ketamine-anaesthetized rat and in absence of general anaesthesia (Haiss and Swarz, 2005).

The complex movements elicited by the long trains of electrical pulses likely activate complex circuits locally about on the electrode tip and in projection sites that includes neurons in a number of cortical and subcortical structures. The manner in which extracellular current activate complexly organized neural tissues is only partly understood. Basically, 3 interdependen aspects have to be considered to understand the effect electrical stimulation have within the nervous tissue. First, the exact extent and shape of the directly activated brain area has to be known. There is a vast literature on the neural elements activated by electrical microstimulation (e.g., Ranck, 1975; Doty and Bartlett, 1981; Yeomans, 1990; Tehovnik, 1996; Rattay, 1999). Despite this, we still know very little about the local and distal brain circuits recruited during the delivery of currents to brain tissue. It is a generally accepted simple rule that electrical microstimulation leads to a sphere of activated neurons around the electrode tip that increases in size with the increasing current so that larger currents activate neurons at a larger distance from the electrode (Stoney *et al.*, 1968; Theovnik *et al.*, 1996; Tolias *et al.*, 2005). In early ICMS studies a single stimulation protocol with single-cell recording was used to deduce the current spread and the direct excitability of pyramidal neurons

within motor cortex of cat (Asanuma *et al.*, 1976; Stoney *et al.*, 1968). It has been estimated that 200 μs pulses with 10 and 100 μA amplitude activate cells in a radius of 100 and 450 μm around the electrode (Stoney *et al.*, 1968). The second problem to be considered is which different neuronal part like dendrites, somata, and axons to be directly activated. The direct excitability (chronaxie) of cortical neurons expressed as the pulse duration at twice of rheobase current was found ranging between 0.1 and 0.4 ms (Asanuma *et al.*, 1976; Stoney *et al.*, 1968). Axons have shorter chronaxies than those of cells bodies and large myelinated axons have shorter chronaxies than those of small, non-myelinated axons (Ranck, 1975). According to these experiments, it is accepted that using 0.2 ms pulses of current the sites of direct activation of cortical neurons are the initial segment and nodes of Ranviers of large myelinated axons (Jankowska *et al.*, 1975; Nowak and Bullier 1998, I,II; Rattay, 1999). Some investigators have used behavioural methods to estimate the spread of electrical stimulation within neocortex (Murasugi *et al.*, 1993; Tehovnik *et al*., 2004 and 2005). Theovnik *et al.* (2004) found that the amount of V1 tissue activated with 50-100 μA current (with 100 ms trains using 0.2 ms pulse delivered at 200 Hz), was estimated to be 0.572 and 0.736 mm, respectively, from the electrode tip and the chronaxie of exited elements ranged between 0.1 and 0.4 ms. Recently, fMRI (functional Magnetic Resonance Imaging) that relies on the BOLD (Blood Oxygen Level-Dependent) signal was used to study the spread properties of electrical stimuli delivered to V1 cortex in anesthetized monkey (Tolias *et al*., 2005). These experiments found that for current levels of 159 to 1,651 (4 sec train duration of 0.2 ms pulses at 100 Hz) the amount of activated tissue ranged from 2 to 4.5 mm from the electrode tip. This extensive spread of current as measured with fMRI is consistent with the spread observed using optical imaging of neocortex where lower currents were used (Seidemann *et al.*, 2002). In other word, electrophysiological, behavioural and imaging methods produced very similar chronaxie values that fell between 0.1 and 0.4 ms, by contrast, they produced different current spread estimates for cortical stimulation. Specifically, electrophysiological and behavioural methods yielded estimates of activity spread that were comparable and imaging methods yielded estimates roughly fourfold greater than those

observed using other methods (for review see Theovnik *et al.*, 2006). A main reason that could account for the observed difference between imaging data and other measures of current spread might be related to transynaptic activity that imaging techniques are able to direct visualize. This insight represents the third problem to be solved: the direct activation of the somata is mated with axonal excitation carrying the activation by ortho-antidromic conveyance of spikes on interconnected structure (indirect effects). Because axons are abundant in neocortex, local antidromic and synaptic effects must be expected to carry the major part of the stimulation effect, especially using long-duration protocol of stimulation. Indeed, it is well established that even single electrical pulse delivered to cortical tissue is able to activate trasynaptically cortical neurons beyond the site of direct stimulation (Asanuma and Rosen, 1973; Jankowska *et al.*, 1975; Butovas and Schwarz, 2003). The transynaptic activation as measured with imaging techniques may be dominated by subthreshold responses (Mathiesen *et al.*, 1998; Logothetis *et al*., 2001) or might also indicate the presence of spiking activity. The lateral spread of the fMRI response beyond of the local direct stimulation might be related to the activation of local horizontal connections and cortico-cortica and/or sub-corticall projections. Recently, results suggest that electrical stimulation of cortex elicited positive BOLD responses in topographically matched regions of cortex all of which are monosynaptic targets of the stimulated site (Tolias *et al.*, 2005) and evidenced for the lack of electrically induced polysynaptic propagation of activity in the neocortex (Sultan *et al.*, 2011). Despite this large number of investigation on ICMS, there is only coarse information about the location of the activated cortical neurons and their distribution at a distance from the stimulating electrode tip. Recent data on cortical excitation with microelectrode has shed new insight on mechanisms involved in ICMS evoked movements. From past studies, using optical technique imaging (Smetter *et al.*, 1999; Stosiek *et al.*, 2003), it know that somatic calcium in cortical neurons largely reflects action potential firing, rather than sub-threshold events. In vivo cortical networks experiments, the 2-photon imaging technique allows for direct imaging of hundreds of activated cortical neurons around the electrode tip (Sato *et al.*, 2007; Kerr and Denk, 2008). Using this

technique it was found that intracortical microstimulation directly activates a sparse, distributed population of neurons around the electrode even at low currents (Histed *et al.*, 2009). The stimulation protocols used by Histed and coll. matched protocols used in previous studies of the influence of cortical circuits on behaviour and also partially matched the protocol of stimulation used in our experiments. They used constant-current biphasic square pulses, each phase lasting 200 μs, with the negative pulse first (Theovnik, 1996) at 250 Hz in trains of 100 to 814 ms at low ($\leq$ 10 μA) currents. The cortical stimulation near threshold produces a sparse and distributed set of activated cells in a way that a small fraction of all neurons were activated. Some of activated neurons were located hundreds of microns away from the electrode tip, while other nearby cells did not respond (Histed *et al.*, 2009). Well known electrophysiological data support the idea that axons near the electrode tip are the main neural elements activated by threshold current stimulation (Theovnik *et al.*, 2006). Histead and coll. suggest that the sparse patterns of activated cell observed at threshold were largely independent of synaptic transmission. According with this conclusion, the pattern of activated cells depend strongly on electrode position in a way that moving the electrode tip 30 μm almost completely eliminated overlap of activated neurons. Activating processes near the tip gives a ball of activated cells, but even near threshold this ball is sparse. Larger currents recruit more neurons, producing greater postsynaptic summation to result in postsynaptic spiking (Stoney *et al.*, 1968; Butovas and Schwarz, 2003) so that increasing current instead of activating cells at greater distance causes the ball to fill in as more cells are activated.

The neocortex contains several excitatory and inhibitory neurons that are complexly interconnected locally as well as over large distances (Braitemberg and Schüz, 1998). This high interconnectivity of the neocortex suggest that a close correlation of both excitatory and inhibitory effects were induced after electrical stimulation. The common finding was that a postsynaptic sequence of fast excitation and long-lasting inhibition response of neocortex has been demonstrated after intracortical microstimulation (Asanuma and Rosén, 1973; Shao and Burkhalter, 1996; Chung and Ferster, 1998; Butovas and Schwarz, 2003; Logothetis *et al.*, 2010). Recentely the effects of

microstimulation on cortical elements was better understood using a multielectrode recordings (Butovas and Schwarz, 2003). Assessing spatial electrical parameters of the stimulation indicated that stimulation frequencies at > 20 Hz evoked repetitive excitatory responses standing out against a continuous background of inhibition. The inhibitory response that follows the fast excitatory response was remarkably static in its temporal characteristics indeed, it is unaffected by stimulus parameters and its takes > 100 ms beyond the duration of the stimulus (Butovas and Schwartz, 2003). These features suggested that it is the activation of synaptic inhibition mediated by GABAb receptor that plays a major role in generating prolonged inhibition after stimulation (Butovas *et al.*, 2006). All these new technical studies are useful to recast the interpretation of studies that used microstimulation to affect cortical activity, and can address the interpretation of our results.

4.2 Why long-duration ICMS of the forelimb motor cortex evoked patterns of coordinated movement

Stimulation of the cortex is non-physiological, and thus the results should be taken cautiously. However, ICMS experiments exposed above can be helpful in explaining why long-duration ICMS of the forelimb motor cortex evoked coordinated movement responses. Moreover, it is important to consider whether the complex movement elicited by long-duration ICMS reflect the activation of motor networks associated with behavioral relevant movements. Typically, in the present experiments at each cortical site, the stimulating current was increased gradually until a clear multijoint movement of the forelimb was detected (current threshold for movement, see Methods). Thus, our explanation for this is that threshold currents recruit neurons, producing postsynaptic summation (Stoney *et al.*, 1968; Butovas and Schwarz, 2003) that resulted in a multijoint forelimb movement evoked 50% of the time. Increasing current to about twice threshold (100 μA), instead of activating cells at greater distance, probably caused the activation of more cells around electrode tip (Histed *et al.*, 2009) and so, a clear, consistent, multijoint movement of the limb was obtained for recording. In rat motor cortex horizontal projections extending laterally by 0.5 to 1 mm could

concur to the lateral spread of electrical response beyond the fringe of direct stimulation. Thus, we can suppose that in our experiments the mechanism of activation was local with a focus on transynaptic effects so that moving the electrode by 500 μm changed the pattern of activate neurons (Histed *et al.*, 2009). It is possible that the ICMS-evoked complex movement may be caused by the activity of a neuronal population significantly larger than neurons activated directly as a result of the passive spread of current. Yet it is possible that ICMS as used in the present experiments activates directly the most excitable elements of the motor cortex and that these elements tend to project to other cortical areas as well as subcortical networks, connected monosynaptically to the direct excited neurons (Logothetis *et al.*, 2010) and involved in the generation of the forelimb movements. Some authors (Strick, 2002) have argued that the long-duration ICMS may lead to nonspecific current spread, generating complex movements by randomly activating a large number of spinal motorneurons. According to this interpretation, the nonspecific and randomly activated spinal motor neuron would result in massive, stereotyped movements, most similar to massive contractions during local or general seizures than to those of voluntary action. Alternatively, if the random activation of multiple simple movements contributing to a complex sequence one would expect that the order of movement in sequences also would be random based on the pseudorandom activation of neurons within the motor cortex. Moreover, long stimulus patterns at high frequencies, as used in the present study, have been shown to elicit a strong and continuous inhibition in neurones residing within a large area surrounding the electrode that could limit the current spread from the stimulation site (Chung and Ferster, 1998; Butovas and Schwarz, 2003). In all our experiments, the long-duration ICMS evoked sequential activation of groups of muscles that shape reproducible patterns of forelimb movements. As in other similar results (Graziano *et al.*, 2002; Ramanathan *et al.*, 2006; Gharbawie *et al.*, 2011), several aspect of our results, suggest that the stimulation-evoked movements may mimic normal one, indeed, in all recorded cases, the movement appeared to be natural and coordinated and we never evoked twisted or unnatural patterns of movement. Thus, we can conclude that the movement appeared to be natural because long-duration

ICMS probably recruits neurons in many parts of the motor-sensory networks and this recruitment of neurons presumably occurs every time we make a natural movement at the same time scale.

One of more interesting result of this study, indicates that in the 50% of stimulated sites, ICMS evoked coordinated forelimb movements involving proximal (shoulder and elbow) and distal (wrist and digit) segments. These sites were dispersed over the forelimb motor region, that is in the proximal as well as in distal forelimb motor area. In rats, the C8 spinal cord segment contains lower motor neurons that activate muscles controlling distal forelimb movements required for grasping, whereas motor neuron pools located in the C4 spinal segment are associated with control of proximal forelimb, shoulder and neck musculature (McKenna *et al.*, 2000). There was abundant evidence that neurons related to distal and proximal actions intermingle considerably within M1 in both primate (Donoghue *et al.*, 1992; McKiernan *et al.*, 1998; Park *et al.*, 2001) and rat (Wang *et al.*, 2011) and that neuron population in a small region of M1 can encode information related to kinematic variables of naturalistic movement of the upper limb (Vargas-Irwin *et al.*, 2010). Within the rat's motor cortex, both C8- and C4-projecting neurons are anatomically distributed throughout the forelimb region, describing an interspersed network of motor neurons that do not collateralize across the C4 and C8 spinal segments (Wang *et al.*, 2011). Our results support the notion that distal forelimb-projecting and proximal forelimb-projecting neurons are intermingled within motor cortex, and could suggest that corticospinal motor neurons were segregated on the basis of their contribution to specific aspect of motor control during naturalistic movements. In rats descending pathways from motor cortex terminate largely on interneurons in the intermediate zone of the spinal cord and lack substantial direct input to motoneurons (Catsman-Berrevoets and Kuypers, 1981). Indeed, it is a common point of view, that the rat's cortico-spinal system utilizes the integrative mechanisms of the spinal cord to generate a range of skilled motor behaviour. Our observations suggest that the activation of proximal and distal segments in ICMS-evoked complex forelimb movement may occur directly within the activated motor cortex. This interpretation do not exclude

that subcortical networks (cerebellum, basal ganglia, and spinal circuits) could be involved in the sequential activation of groups of muscles in electrically evoked forelimb movements.

5. Figures

Tab. 1 Wrist marker maximum displacement (MD)

Class	MD X(mm)	MD Y(mm)	MD Z(mm)
$ab_{n=98}$	5.53 ± 0.83	21.72 ± 0.82	22.99 ± 1.14
$ad_{n=18}$	-2.40 ± 1.65	-10.29 ± 1.42	7.61 ± 1.95
$ex_{n=35}$	19.33 ± 1.45	7.92 ± 0.96	14.61 ± 1.50
$rt_{n=3}$	-10.13 ± 1.67	7.26 ± 0.98	17.01 ± 3.28
$el_{n=23}$	0.76 ± 0.34	3.08 ± 0.26	10.17 ± 0.50

Tab. 1: Mean scores (± SEM) of maximum displacement (MD) in XYZ-axes measured (mm) of the wrist marker classes of movement: *ab*, abduction; *ad*, adduction; *ex*, extension; *rt*, retraction; *el*, elevation; n: number of sites for each class.

Tab. 2 Wrist marker kinematics

Class	L(ms)	D(ms)	MPV(mm/s)	MV(mm/s)	PV(n)	T(mm)	DV(mm)
$ab_{n=98}$	23.46 ± 0.69	506.80 ± 15.20	428.00 ± 18.60	128.70 ± 13.60	2.32 ± 0.08	60.82 ± 3.04	29.15 ± 0.97
$ad_{n=18}$	31.11 ± 2.12	387.20 ± 45.20	476.9 0 ± 41.40	98.60 ± 11.10	1.94 ± 0.22	32.77 ± 2.57	13.91 ± 1.44
$ex_{n=35}$	26.18 ± 1.20	434.90 ± 23.30	492.20 ± 32.10	157.60 ± 12.60	3.97 ± 0.33	82.88 ± 9.23	22.26 ± 1.71
$rt_{n=3}$	23.33 ± 3.33	473.00 ± 107.00	273.6 0 ± 720	77.10 ± 15.70	2.00 ± 0.00	35.50 ± 1.61	20.57 ± 3.23
$el_{n=23}$	26.96 ± 1.47	414.30 ± 36.40	376.40 ± 42.40	70.89 ± 8.85	2.60 ± 0.39	26.05 ± 1.88	11.21 ± 0.54

Tab. 2: Mean scores (± SEM) of kinematic variables of the wrist classes of movement (see caption in Tab. 1). Kinematic variables were: L, movement latency; D, movement duration; MPV, maximum peak velocity; MV, mean velocity; PV, number of peaks velocity; T, trajectory; DV, displacement vector. Units: ms: milliseconds; s: seconds; mm: millimetres; n: numbers.

Tab. 3 Digit marker maximum displacement (MD)

Class	MD X(mm)	MD Y(mm)	MD Z(mm)
$O_{n=82}$	9.90 ± 0.38	4.75 ± 0.31	9.35 ± 0.25
$C_{n=7}$	-12.97 ± 0.38	6.90 ± 0.91	10.46 ± 1.18
$OC_{S\ n=12}$ opening phase	9.49 ± 1.01	3.32 ± 0.65	9.80 ± 0.51
$OC_{S\ n=12}$ closing phase	-6.45 ± 0.88	-2.38 ± 0.60	-9.93 ± 0.47
$S_{n=23}$	2.75 ± 0.82	-2.10 ± 1.00	4.06 ± 0.18

Tab. 3: Mean scores (± SEM) of maximum displacement (MD) in XYZ-axes measured (mm) of the digit marker classes of movement: *O*, opening; *C*, closure; *OCs*, opening/closure sequence (divided into opening phase and closing phase); *S*, supination; n: number of sites for each class.

Tab. 4 Digit marker kinematics

Class	L(ms)	D(ms)	MV(mm/s)	MPV(mm/s)	PV(n)
$O_{n=82}$	29.76 ± 1.18	365.50 ± 13.30	39.70 ± 2.39	357.20 ± 19.50	1.60 ± 0.05
$C_{n=7}$	24.29 ± 2.02	321.43 ± 9.62	68.70 ± 13.80	506.60 ± 15.30	1.57 ± 0.20
$OC_{S\ n=12}$	27.50 ± 1.31	568.30 ± 34.70	84.40 ± 13.40	362.10 ± 37.20	5.58 ± 0.48*
$S_{n=23}$	28.26 ± 1.36	364.35 ± 7.22	15.48 ± 2.20	149.60 ± 38.40	1.65 ± 0.10

Tab. 4: Mean scores (± SEM) of kinematic variables of the digit classes of movement (see caption in Tab. 3). Kinematic variables were: L, movement latency; D, movement duration; MPV, maximum peak velocity; MV, mean velocity; PV, number of peaks velocity. Units: see Tab. 2

Fig. 1

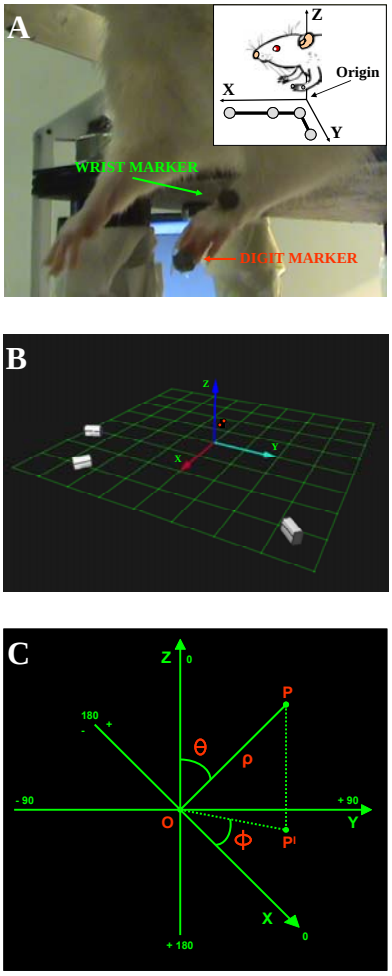

Fig. 1 (A-C): Illustration of markers, Qualisys System set up and Spherical Coordinate System. **A:** Placement of the reflective markers and forelimbs resting position hanging free. The stationary L-shaped reference structure (top right box) with its 4 markers defined the origin and orientation of the coordinate system. **B:** Qualisys software reconstruction of the real experimental space in which it is showed the real cameras and markers position. The 3 cameras were placed to allow the detection of markers simultaneously from each camera. The suspended circles were the 2 markers. **C:** Spherical coordinate system is illustrated for the 3D evaluation of movement direction. Spherical coordinates of a given point P in the XYZ space were defined as follows: *rho (ρ)*: was the distance between P and O. In present data ρ was the movement vector; all vectors were made to origin from the intersection of axes. *phi (φ)*: was the angle between the positive X-axis and OP^{I}; counter clockwise was considered the positive direction (φ: between 0 and ± 180°). *theta (θ)*: was the angle between the Z-axis and OP (θ: between 0 and 180°).

Fig. 2

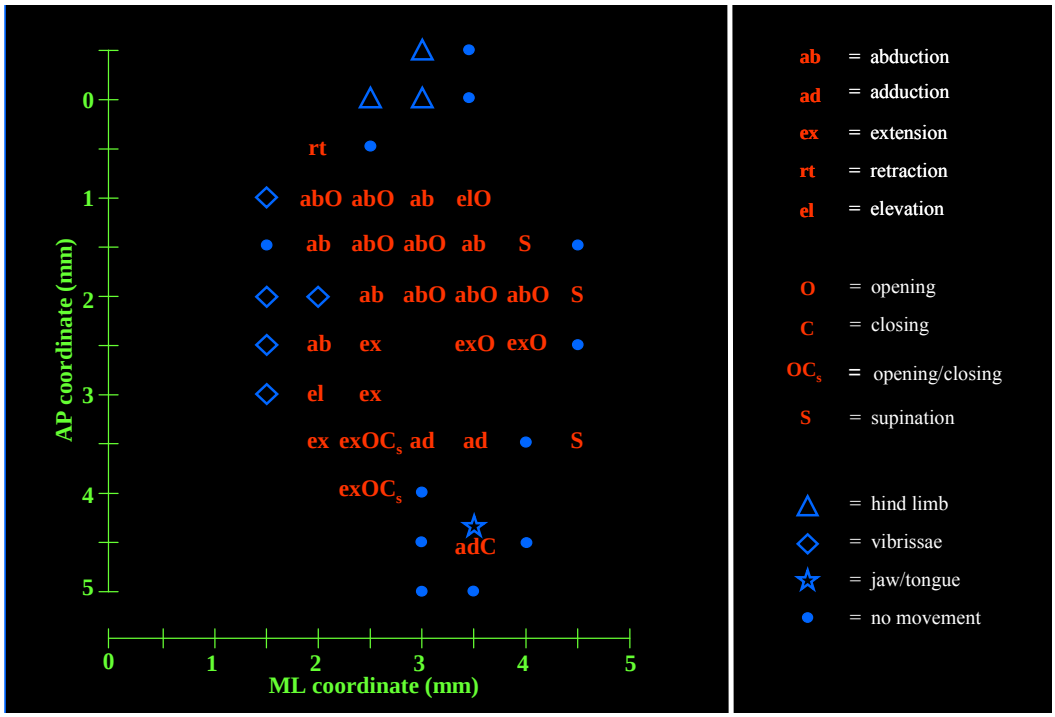

Fig. 2: Representative motor map derived by using the long-duration ICMS paradigm, demonstrating the complex movement representations. Interpenetration distances were 500 µm. The microelectrode was sequentially introduced to a depth of 1500 µm and movements were evoked with stimulation intensity of 100 µA. In this M1 mapping scheme, frontal pole was at the bottom and 0 corresponded to bregma; numbers indicated rostral or caudal distance from the bregma or lateral distance from the midline.
Legend explanation:

- Lowercase letter, wrist marker movements: *ab*, abduction; *ad*, adduction; *ex*, extension; *rt*, retraction; *el*, elevation;
- Uppercase letter, digit marker movements: *O*, opening; *C*, closure; *OCs* opening/closing sequence; *S*, supination;
- Symbols, site where no forelimb movement was evoked: open diamond, vibrissae or neck; open triangle, hindlimb; open star, jaw-tongue; small filled circle, site unresponsive at 100 µA;
- No symbol: penetration not performed due to presence of large vessel;
- Non-forelimb movement observed simultaneously with forelimb movements was not showed, except the opening mouth movement (open star);

In all rat forelimb responses could be elicited within a maximum distance of 0.5-4.5 mm anterior and 1.5-4.5 mm lateral. In this map, the caudal and rostral forelimb areas were not well separated from each other by a region associated with vibrissae and neck movements.

Fig. 3

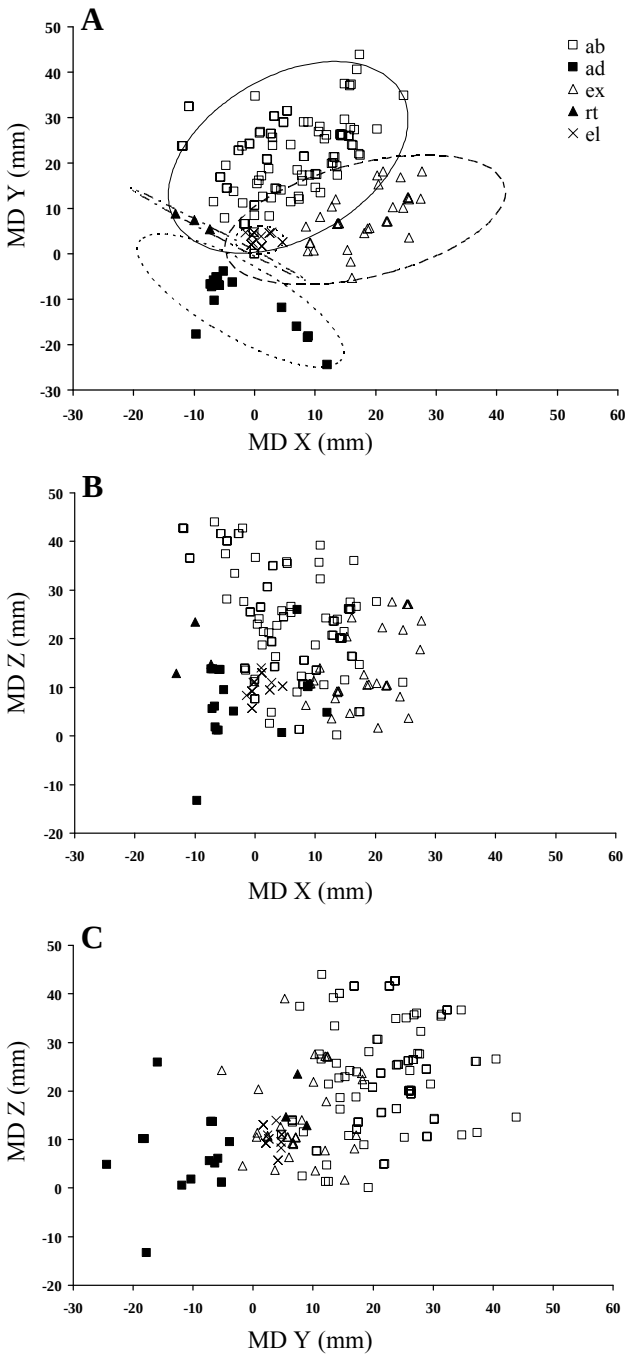

Fig. 3 (A-C): Description of limb movements according to maximum displacement (MD). Scatter plot displaying MD in XYZ-axes for all of the wrist marker movements for different animals. Individual data were represented by point markers in 2D space, where axes represent the variables: (**A:** X vs Y; **B:** X vs Z; **C:** Y vs Z). Movement class is symbol coded as: *ab*, abduction; *ad*, adduction; *ex*, extension; *rt*, retraction; *el*, elevation. The plot in **A** visualized the class of movements as a cluster of points highlighted by the confidence ellipsoids (95% confidence limits, Proportion Correct = 0.85) conversely, the plot in **B** and **C** lacked of clear clustering (Proportion Correct = 0.60 and 0.75 respectively). This suggest that the movement class discrimination was more related to the marker's displacement along X and Y axes.

Fig. 4

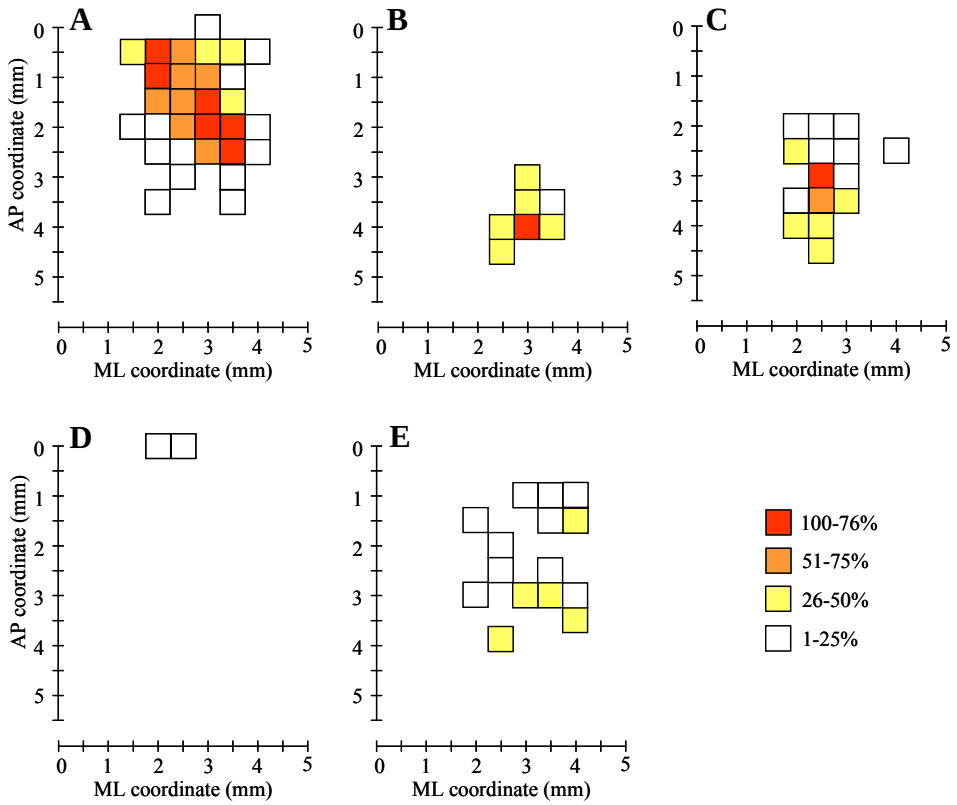

Fig. 4 (**A-E):** Description of limb movements according to the distribution of sites across cortical surface. Surface plot showing the frequency distribution of limb sites at each coordinate relative to bregma (animal n = 7, sites n = 177). 100% of probability is achieved when a movement at that site was observed in all 7 animals. Specifically, the *ab* sites were found almost in all animals between 0.5-2.5 mm anterior and 2-3.5mm lateral to bregma (**A**); whereas the *ad* sites were found between 3-4.5 mm anterior and 2.5-3.5 mm lateral to bregma (**B**). The *ex* sites were found between 2-4.5 mm anterior and 2-3 mm lateral to bregma (**C**); whereas the *rt* movement was found at bregma and 2-2.5 mm lateral to bregma (**D**). Unlike to other sites, *el* sites were widespread throughout the limb motor region (**E**).

Fig. 5

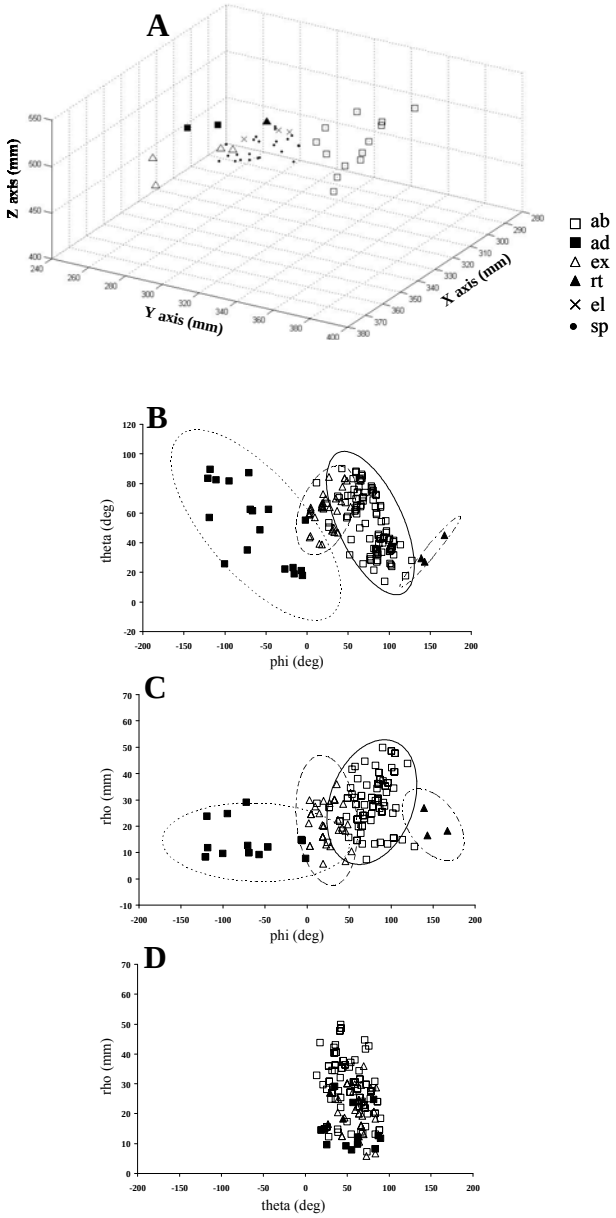

Fig. 5 (**A-D):** Description of limb movements according to the limb location in space. Classes of movement were symbol coded as showed in Fig. 3, while small full dots were the starting points (sp). **A:** Example of MATLAB 3D plot (see Appendix) of final limb end-point locations evoked in one animal. Final end-point locations were different for each class of movement. Note that the scales were different for each axis to improve legibility. **B-D:** 2D scatter plot of spherical coordinates showing the movement end-point locations across animals. Since *el* movements were carried out only vertically upwards on Z-axis (MD in X and Y axes < 5 mm), they were not displayed in these plots. Plot **B** (*phi* vs *theta*) and **C** (*phi* vs *rho*) showed end-points according to the azimuthal component of movement (*phi* angle, longitude around head-chest fixed position). Plot **D** (*theta* vs *rho*) showed end-points according to the zenithal component of movement (*theta* angle, latitude around head-chest fixed position). Plot **B** and **C** visualized the movements end-point as a cluster of points highlighted by the confidence ellipsoids (95% confidence limits, Proportion Correct = 0.68 and 0.75 respectively) conversely, plot **D** was lacked of clear clustering (Proportion Correct = 0.52). This suggest that *phi* angle was crucial in order to discriminate movement class and also that all animals had nearly similar spatial organization of the limb movements.

Fig. 6

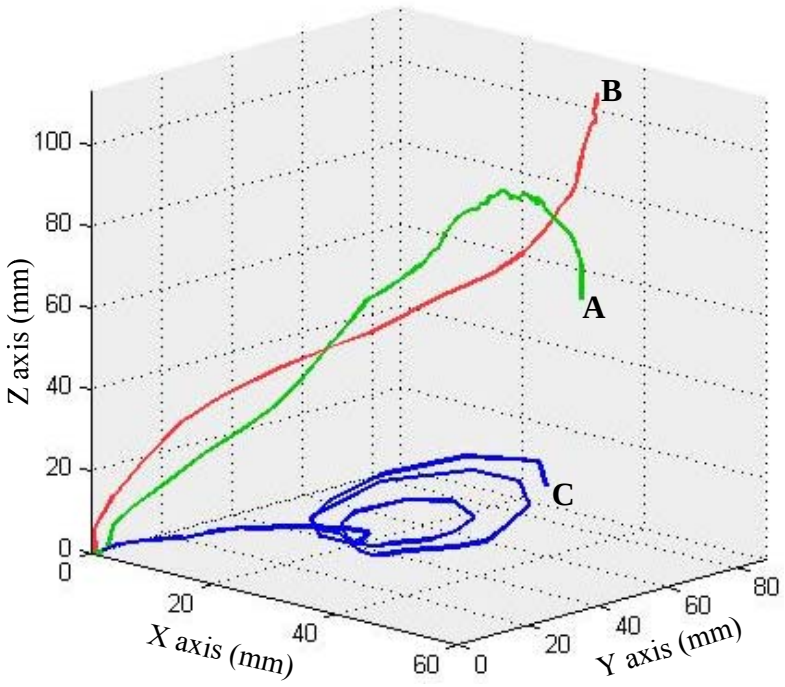

Fig. 6: MATLAB 3D representation (see Appendix) of trajectories with path index > 1.57 and different shape. **A:** C-shaped; **B:** S-shaped; **C:** coil-like-shaped. Coil-like-shaped trajectory was found in 25.7% of extension-related sites. All trajectories began at (0,0,0). Note that the scales are not equivalent on each axis of the figure, which improves the legibility of the graph but artificially decrease the curvature impression (Z-axis has been less expanded).

Fig. 7

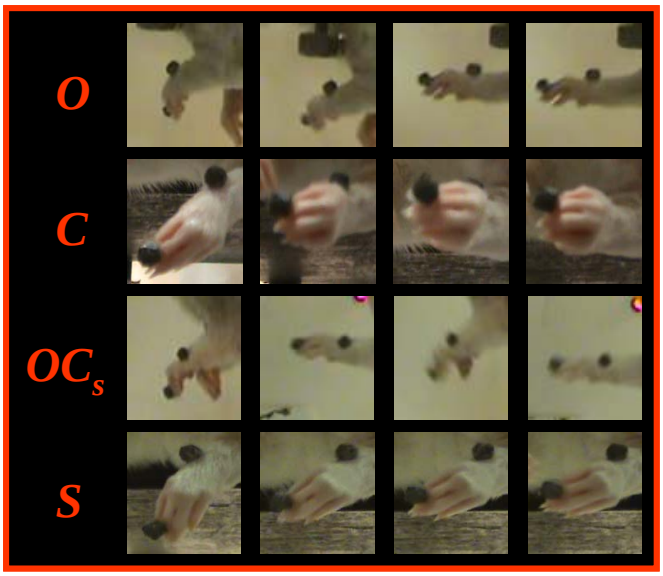

Fig. 7: Paw movements elicited by long-duration ICMS within motor cortex. Sequences of pictures taken from a video recording when paw movement was elicited. In each sequence, the picture on the left shows the position of the paw at the beginning of the movement (0 ms), in others the position of the paw was in steps of 180 ms. 4 classes of paw movements were identified: paw opening (*O*), paw closure (*C*), paw opening/closing sequence (*OCs*), paw supination (*S*). *O*, *C*, and *OCs* movements characterized by contraction of all digits simultaneously. The paw opening/closing sequence characterized by repetitive sequences in each single trial. *S* movement characterized by external rotation of the wrist without moving fingers.

Fig. 8

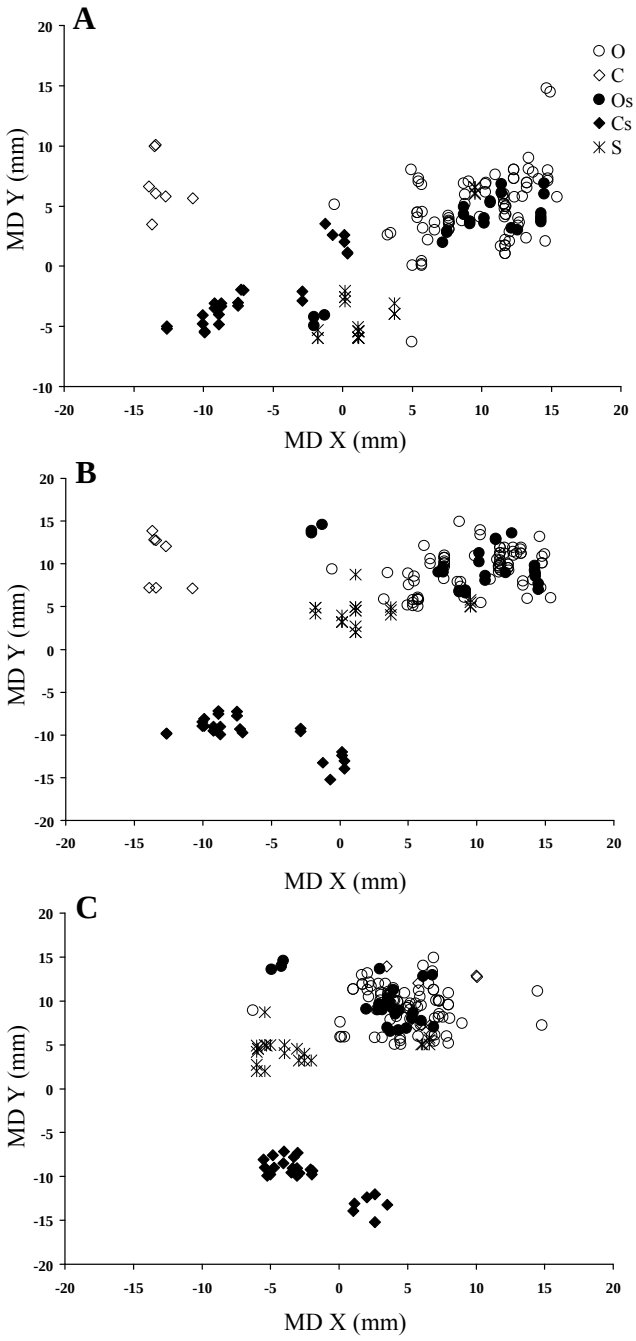

Fig. 8: Description of paw movement according to maximum displacement (MD). Scatter plot displaying MD in XYZ-axes for all of the digit marker movements for different animals. Individual data were represented by point markers in 2D space, where axes represent the variables: (**A:** X vs Y; **B:** X vs Z; **C:** Y vs Z). Movement class is symbol coded as: *O*, opening; *C*, closure; *OCs*, opening/closing sequence; *S*, supination. Notably, the overlap of *O* and *OCs* opening phase points in all 3 plots and the clustering of *C* and *OCs* closing phase points in plots **A** and **B**.

Fig. 9

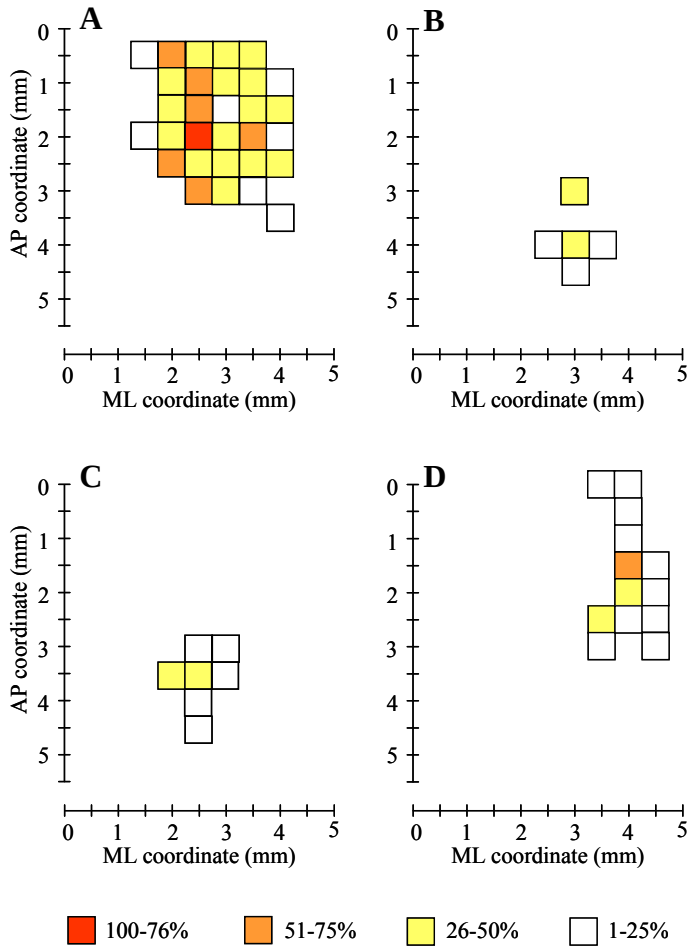

Fig. 9 (A-D): Description of paw movements according to the distribution of sites across cortical surface. Surface plot showing the frequency distribution of paw movements (*O*, *C*, *O/Cs*, *S*) at bregma relative coordinates (animal n = 7, sites n = 124). The frequency of paw movements is coded by different gray levels as in Fig.4. Specifically, the paw opening was found between 0.5-3 mm anterior and 2-4 mm lateral to midline (**A**); whereas the paw closure was found between 3-4.5 mm anterior and 3-4 mm lateral to midline (**B**). The paw open-closure sequence was found between 3-4.5 mm anterior and 3-4 mm lateral to midline (**C**). The paw supination was found between 0-3.5 mm anterior and 3.5-4.5 mm lateral to midline (**D**).

6. References

Adamovich SV, Archambault PS, Ghafouri M, Levin MF, Poizner H, Feldman AG (2001) Hand trajectory invariance in reaching movements involving the trunk. Exp Brain Res. 138(3): 288-303

Archambault P, Pigeon P, Feldman AG, Levin MF (1999) Recruitment and sequencing of different degrees of freedom during pointing movements involving the trunk in healthy and hemiparetic subjects. Exp Brain Res. 126(1): 55-67

Asanuma H, Rosén I (1973) Spread of mono- and polysynaptic connections within cat's motor cortex. Exp Brain Res. 16(5): 507-20

Asanuma H, Arnold AP (1975) Noxious effects of excessive currents used for intracortical microstimulation. Brain Res. 96(1): 103-7

Asanuma H, Arnold A, Zarzecki P (1976) Further study on the excitation of pyramidal tract cells by intracortical microstimulation. Exp Brain Res. 26(5): 443-61

Barker TM, McCombe P (1999) Discriminant analysis of human kinematic data: application to human lumbar spinal motion. Proc Inst Mech Eng H. 213(6): 447-53

Bartlett JR Doty RW (1981) An exploration of the ability of macaques to detect microstimulation of striate cortex. Acta Neurobiol Exp (Wars). 40(4): 713-27

Braitenberg V, Schüz, A (1998) Cortex: Statistics and geometry of neuronal connectivity: Springer Berlin

Brecht M, Krauss A, Muhammad S, Sinai-Esfahani L, Bellanca S, Margrie TW (2004) Organization of rat vibrissa motor cortex and adjacent areas according to cytoarchitectonics, microstimulation, and intracellular stimulation of identified cells. J Comp Neurol. 479(4): 360-73

Bruce CJ, Goldberg ME, Bushnell MC, Stanton GB (1985) Primate frontal eye fields. II. Physiological and anatomical correlates of electrically evoked eye movements. J Neurophysiol. 54(3): 714-34

Butovas S, Schwarz C (2003) Spatiotemporal effects of microstimulation in rat neocortex: a parametric study using multielectrode recordings. J Neurophysiol. 90(5): 3024-39

Butovas S, Hormuzdi SG, Monyer H, Schwarz C (2006) Effects of electrically coupled inhibitory networks on local neuronal responses to intracortical microstimulation. J Neurophysiol. 96(3): 1227-36

Capaday C, Devanne H, Bertrand L, Lavoie BA (1998) Intracortical connections between motor cortical zones controlling antagonistic muscles in the cat: a combined anatomical and physiological study. Exp Brain Res. 120(2): 223-32

Catsman-Berrevoets CE, Kuypers HG (1981) A search for corticospinal collaterals to thalamus and mesencephalon by means of multiple retrograde fluorescent tracers in cat and rat. Brain Res. 218(1-2): 15-33

Chung S, Ferster D (1998) Strength and orientation tuning of the thalamic input to simple cells revealed by electrically evoked cortical suppression. Neuron. 20(6): 1177-89

Donoghue JP, Wise SP (1982) The motor cortex of the rat: cytoarchitecture and microstimulation mapping. J Comp Neurol. 212(1): 76-88

Donoghue JP, Leibovic S, Sanes JN (1992) Organization of the forelimb area in squirrel monkey motor cortex: representation of digit, wrist, and elbow muscles. Exp Brain Res. 89(1): 1-19

Donoghue JP (1995) Plasticity of adult sensorimotor representations. Curr Opin Neurobiol. 5(6): 749-54

Ebert B, Mikkelsen S, Thorkildsen C, Borgbjerg FM (1997) Norketamine, the main metabolite of ketamine, is a non-competitive NMDA receptor antagonist in the rat cortex and spinal cord. Eur J Pharmacol. 333(1): 99-104

Franchi G (2000) Reorganization of vibrissal motor representation following severing and repair of the facial nerve in adult rats. Exp Brain Res. 131(1): 33-43

Freedman EG, Stanford TR, Sparks DL (1996) Combined eye-head gaze shifts produced by electrical stimulation of the superior colliculus in rhesus monkeys. J Neurophysiol. 76(2): 927-52

Gharbawie OA, Stepniewska I, Qi H, Kaas JH (2011) Cortical connections of functional zones in posterior parietal cortex and frontal cortex motor regions in new world monkeys. Cereb Cortex. 21(9): 1981-2002

Gharbawie OA, Stepniewska I, Qi H, Kaas JH (2011) Multiple parietal-frontal pathways mediate grasping in macaque monkeys. J Neurosci. 31(32): 11660-77

Gottlieb JP, Bruce CJ, MacAvoy MG (1996) Smooth eye movements elicited by microstimulation in the primate frontal eye field. J Neurophysiol. 69(3): 786-99

Graziano MS, Taylor CS, Moore T (2002) Complex movements evoked by microstimulation of precentral cortex. Neuron. 34(5):841-51

Graziano MS, Taylor CS, Moore T, Cooke DF (2002) The cortical control of movement revisited. Neuron. 36(3): 349-62

Graziano MS, Taylor CS, Moore T (2002) Probing cortical function with electrical stimulation. Nat Neurosci. 5(10): 921

Graziano MS, Aflalo TN, Cooke DF (2005) Arm movements evoked by electrical stimulation in the motor cortex of monkeys. J Neurophysiol. 94(6): 4209-23

Haiss F, Schwarz C (2005) Spatial segregation of different modes of movement control in the whisker representation of rat primary motor cortex. J Neurosci. 25(6): 1579-87

Histed MH, Bonin V, Reid RC (2009) Direct activation of sparse, distributed populations of cortical neurons by electrical microstimulation. Neuron. 63(4): 508-22

Jankowska E, Padel Y, Tanaka R (1975) The mode of activation of pyramidal tract cells by intracortical stimuli. J Physiol. 249(3): 617-36

Kartje-Tillotson G, Neafsey **EJ, Castro AJ (1985)** Electrophysiological analysis of motor cortical plasticity after cortical lesions in newborn rats. Brain Res. 332(1): 103-11

Kayama Y, Iwama K (1972) The EEG, evoked potentials, and single-unit activity during ketamine anesthesia in cats. Anesthesiology. 36(4): 316-28

Kerr JN, Denk W (2008) Imaging in vivo: watching the brain in action. Nat Rev Neurosci. 9(3): 195-205

Linton LR, Harder LD (2007) Biology 315 – Quantitative Biology Lecture Notes. University of Calgary, Calgary, AB

Logothetis NK, Pauls J, Augath M, Trinath T, Oeltermann A (2001) Neurophysiological investigation of the basis of the fMRI signal. Nature. 412(6843): 150-7

Logothetis NK, Augath M, Murayama Y, Rauch A, Sultan F, Goense J, Oeltermann A, Merkle H (2010) The effects of electrical microstimulation on cortical signal propagation. Nat Neurosci. 13(10): 1283-91

Lowry R (2008) One Way ANOVA – Independent Samples. Vassar.edu.

Mathiesen C, Caesar K, Akgören N, Lauritzen M (1998) Modification of activity-dependent increases of cerebral blood flow by excitatory synaptic activity and spikes in rat cerebellar cortex. J Physiol. 512 (Pt 2): 555-66

McKenna JE, Prusky GT, Whishaw IQ (2000) Cervical motoneuron topography reflects the proximodistal organization of muscles and movements of the rat forelimb: a retrograde carbocyanine dye analysis. J Comp Neurol. 419(3): 286-96

McKiernan BJ, Marcario JK, Karrer JH, Cheney PD (1998) Corticomotoneuronal postspike effects in shoulder, elbow, wrist, digit, and intrinsic hand muscles during a reach and prehension task. J Neurophysiol. 80(4): 1961-80

Murasugi CM, Salzman CD, Newsome WT (1993) Microstimulation in visual area MT: effects of varying pulse amplitude and frequency. J Neurosci. 13(4): 1719-29

Nowak LG, Bullier J (1998) Axons, but not cell bodies, are activated by electrical stimulation in cortical gray matter. I. Evidence from chronaxie measurements. Exp Brain Res. 118(4): 477-88

Nowak LG, Bullier J (1998) Axons, but not cell bodies, are activated by electrical stimulation in cortical gray matter. II. Evidence from selective inactivation of cell bodies and axon initial segments. Exp Brain Res. 118(4): 489-500

Park MC, Belhaj-Saïf A, Gordon M, Cheney PD (2001) Consistent features in the forelimb representation of primary motor cortex in rhesus macaques. J Neurosci. 21(8): 2784-92

Ramanathan D, Conner JM, Tuszynski MH (2006) A form of motor cortical plasticity that correlates with recovery of function after brain injury. Proc Natl Acad Sci U S A. 103(30): 11370-5

Romo R, Hernández A, Zainos A, Salinas E (1998) Somatosensory discrimination based on cortical microstimulation. Nature. 392(6674): 387-90

Ranck JB Jr (1975) Which elements are excited in electrical stimulation of mammalian central nervous system: a review. Brain Res. 98(3): 417-40

Rattay F (1999) The basic mechanism for the electrical stimulation of the nervous system. Neuroscience. 89(2): 335-46

Salzman CD, Britten KH, Newsome WT (1990) Cortical microstimulation influences perceptual judgements of motion direction. Nature. 346(6280): 174-7

Sato TR, Gray NW, Mainen ZF, Svoboda K (2007) The functional microarchitecture of the mouse barrel cortex. PLoS Biol. 5(7): e189

Schieber MH (2001) Constraints on somatotopic organization in the primary motor cortex. J Neurophysiol. 86(5): 2125-43

Schneider D, Schneider L, Claussen CF, Kolchev C (2001) Cortical representation of the vestibular system as evidenced by brain electrical activity mapping of vestibular late evoked potentials. Ear Nose Throat J. 80(4): 251-2, 255-8

Seidemann E, Arieli A, Grinvald A, Slovin H (2002) Dynamics of depolarization and hyperpolarization in the frontal cortex and saccade goal. Science. 295(5556): 862-5

Shao Z, Burkhalter A (1996) Different balance of excitation and inhibition in forward and feedback circuits of rat visual cortex. J Neurosci. 16(22): 7353-65

Smetters D, Majewska A, Yuste R (1999) Detecting action potentials in neuronal populations with calcium imaging. Methods. 18(2): 215-21

Sonner JM, Zhang Y, Stabernack C, Abaigar W, Xing Y, Laster MJ (2003) GABA(A) receptor blockade antagonizes the immobilizing action of propofol but not ketamine or isoflurane in a dose-related manner. Anesth Analg. 96(3): 706-12

Stepniewska I, Friedman RM, Gharbawie OA, Cerkevich CM, Roe AW, Kaas JH (2011) Optical imaging in galagos reveals parietal-frontal circuits underlying motor behavior. Proc Natl Acad Sci U S A. 108(37): E725-32

Stoney SD Jr, Thompson WD, Asanuma H (1968) Excitation of pyramidal tract cells by intracortical microstimulation: effective extent of stimulating current. J Neurophysiol. 31(5): 659-69

Stosiek C, Garaschuk O, Holthoff K, Konnerth A (2003) In vivo two-photon calcium imaging of neuronal networks. Proc Natl Acad Sci U S A. 100(12): 7319-24

Strick PL (2002) Stimulating research on motor cortex. Nat Neurosci. 5(8): 714-5

Sultan F, Augath M, Murayama Y, Tolias AS, Logothetis N (2011) esfMRI of the upper STS: further evidence for the lack of electrically induced polysynaptic propagation of activity in the neocortex. Magn Reson Imaging. 29(10): 1374-81

Tehovnik EJ, Lee K (1993) The dorsomedial frontal cortex of the rhesus monkey: topographic representation of saccades evoked by electrical stimulation. Exp Brain Res. 96(3): 430-42

Tehovnik EJ (1996) Electrical stimulation of neural tissue to evoke behavioral responses. J Neurosci Methods. 65(1): 1-17

Tehovnik EJ, Slocum WM (2004) Behavioural state affects saccades elicited electrically from neocortex. Neurosci Biobehav Rev. 28(1):13-25

Tehovnik EJ, Slocum WM, Schiller PH (2005) Delaying visually guided saccades by microstimulation of macaque V1: spatial properties of delay fields. Eur J Neurosci. 22(10): 2635-43

Tolias AS, Sultan F, Augath M, Oeltermann A, Tehovnik EJ, Schiller PH, Logothetis NK (2005) Mapping cortical activity elicited with electrical microstimulation using FMRI in the macaque. Neuron. 48(6): 901-11

Vargas-Irwin CE, Shakhnarovich G, Yadollahpour P, Mislow JM, Black MJ, Donoghue JP (2010) Decoding complete reach and grasp actions from local primary motor cortex populations. J Neurosci. 30(29): 9659-69

Wang DL, Liu XL, Qiao DC (2011) Changes of subthalamic nucleus and cortex activity in rat during exhausting exercise. Zhongguo Ying Yong Sheng Li Xue Za Zhi. 27(4): 427-31

Yeomans JS (1990) "Temporal summation decay" in hypothalamic self-stimulation: threshold changes at long intrapair intervals due to axonal subnormal periods. Behav Neurosci. 104(6): 991-9

Acknowledgments

Inizio col ringraziare tutte le persone che con la loro infinita disponibilità e la loro indispensabile professionalità mi hanno accompagnata e guidata durante gli anni di dottorato: a ***Stefania Zanellati****,* ***Valerio Muzzioli****,* ***Enrico Lodi****,* ***Riccardo Viaro****,* ***Emma Maggiolini*** *e* ***Claudio Bonifazzi*** *un grazie di cuore.*

Al dottor ***Gianfranco Franchi*** *và un ringraziamento particolare….grazie per le opportunità che mi ha regalato e grazie per tutto ciò che mi ha saputo trasmettere ed insegnare.*

Infine, ringrazio con tutta me stessa la mia semplicemente ***splendida famiglia.***